An Application of Bernoulli's Principle & the Continuity Equation

Leah Gaeta
ME 303: Fluid Mechanics
Lab: Thursday, February 20, 2020 2:00 pm
ltgaeta@bu.edu

March 6, 2020

1 Introduction

In the context of fluid mechanics, often the engineer wants to know how substances flow into and out of a system and which assumptions can be made about the properties of such substances. Of particular importance is the Reynold's Transport Theorem (Eq. 1), which describes the time rate of change of the mass of a system as equal to the time rate of change of the mass of the contents within a system's control volume (cv) plus the net flow rate of mass through the a system's control surface (cs).

$$\frac{D}{Dt}\int\limits_{sys} \rho \, d\forall = \frac{\partial}{\partial t}\int\limits_{cv} \rho \, d\forall + \int\limits_{cs} \rho(\vec{v}\cdot\hat{n}) \, dA \tag{1}$$

Here, ρ is the density and $\vec{v}$ is the velocity of the fluid, while $\hat{n}$, $\forall$, and A represent the normal vector pointing out, the volume, and the area, respectively. The Continuity Equation, which can be derived from Reynold's Transport Theorem when the flow is both steady and incompressible, affirms that the mass flow rate into a system must equal the mass flow rate out of a system (Eq. 2).

$$\dot{m}_{in} - \dot{m}_{out} = \rho \int V_{in} \, dA_{in} - \rho \int V_{out} \, dA_{out} = 0 \tag{2}$$

$$V_{ave,in}A_{in} = V_{ave,out}A_{out} \tag{3}$$

This further simplifies to Eq. 3 where V_{ave} represents the spatial average of the velocity over the cross-sectional area A.

In addition, if one assumes the flow to be inviscid, steady, incompressible, and along a streamline, then Bernoulli's Principle is also applicable. Derived from Newton's Second Law for inviscid fluids (Eq. 4), the Bernoulli equation can be used to relate the pressures, velocities, and vertical positions between two points along a streamline (Eq. 5). From this, one can determine the stagnation pressure at a point along a horizontal because the flow is at rest and there is therefore no velocity. In all, the stagnation pressure, static pressure, and velocity can be related as shown in Eq. 6 while maintaining the necessary assumptions for Bernoulli's Principle.

$$-\nabla P - \rho g\hat{k} = \rho\vec{a} \tag{4}$$

$$P_s + \frac{1}{2}\rho V^2 + \rho g z = constant \tag{5}$$

$$P_t = P_s + \frac{1}{2}\rho V^2 \tag{6}$$

Applying these principles to this experiment, we expect the velocity and pressure to change throughout the wind tunnel as air flows from left to right. Assuming steady and inviscid flow, the velocity will increase as the flow proceeds through the converging duct to the throat, where it will reach its maximum, and then decrease as it flows through the diverging duct. On the other hand, the pressure will behave just opposite, decreasing with decreasing cross-sectional areas through the tunnel, and then increasing through the diverging duct. In addition, instead of taking measurements from every port along the tunnel, we measured only four sections and then applied continuity to determine the

velocities, and therefore also the flow rates, pressures, and Reynold's numbers for the ports not explicitly measured. Velocity can then be used to find a Mach number, which is the velocity divided by the speed of sound (343.21 $\frac{m}{s}$). Any flows with Mach numbers ¡ 0.3 can be considered incompressible flows.

2 Experimental

Before taking measurements at the ports of the wind tunnel, readings of the microtector-manometer and pressure transducer (voltage) were taken with the axial fan off and on for calibration. This will be further discussed in the following section where the formation of a calibration fit line is illustrated. Next, using the Kiel probe, the transducer pressure was read at various vertical positions of Ports 1, 5, 8, and 10. These pressure values represented the differential pressures at these position; that is, the difference between the static and stagnation pressure. Note that the ports varied in horizontal position, with 1 and 5 in the converging duct, 8 at the throat, and 10 in the diverging duct. Finally, the transducer voltage readings were taken at each port so that the static pressures could be calculated at these test sections.

3 Analysis

Prior to beginning all calculations of the velocities and pressures at the ports, the pressure transducer voltage readings with the fan on/off and respective microtector readings were calibrated. Assuming a linear relationship between pressure and voltage of the transducer, a first-degree polynomial fit was made using Eq. 7 and then Eq. 8 , where x is the pressure difference, h_2 and h_0 are the microtector heights with the fan on and off respectively, ρ is the density of the manometer fluid (water), and g is the acceleration due to gravity. Eq. 8 specifically shows the general equation of calibration fitting and the exact equation and fit are displayed in Figure 1.

$$x = 2(h_2 - h_0)\rho g \tag{7}$$

$$V = m(\Delta p) + b \tag{8}$$

After calibrating, the differential pressures and velocities were calculated for the tested ports (1, 5, 8, and 10) by rearranging Eq. 8 to solve for the pressures and using Eq. 9, respectively. Note that in Eq. 8, V is the voltage from the transducer while in Eq. 9, V is the velocity. Here, we took ρ to be the density of air as that was flowing through the wind tunnel; this is measured to be 1.225 $\frac{kg}{m^3}$ for the temperature and pressure of the laboratory. The velocities of the various vertical positions at each of the ports are plotted in Figure 2 below.

The principle of continuity was then used to find the velocities of the different ports that were not measured. First, average velocities were calculated at the tested ports using the trapezoidal method between data points within the respective velocity profiles. An example of this calculation is shown in Eq. 10 where N is the number of data points and y is the velocity at each point. The flow rate, Q = V_{ave}A, was then found at the tested ports using the average velocities. Port 1, 5, and 8 had flow rates of 0.186, 0.171, and 0.185

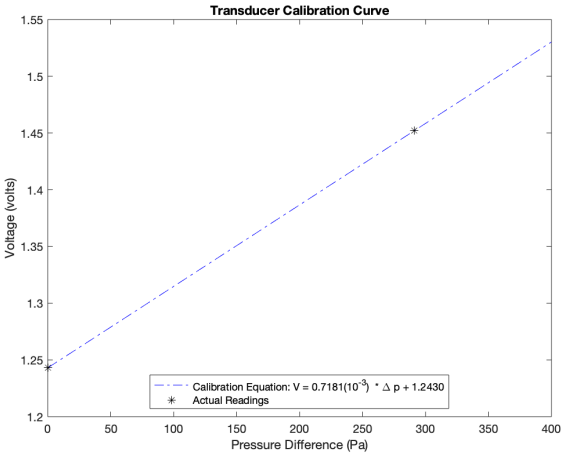

Figure 1: Calibration curve of the pressure found from the readings of the transducer voltage and microtector.

$\frac{m^3}{s}$ while Port 10 had a flow rate of 0.617 $\frac{m^3}{s}$.

$$V = \sqrt{\frac{2(P_t - P_s)}{\rho}} \tag{9}$$

$$V_{ave} = \frac{1}{2(N-1)}[y_1 + 2y_2 + ... + 2y_{N-1} + y_N] \tag{10}$$

$$Re = \frac{\rho V_{ave} D_h}{\mu} \tag{11}$$

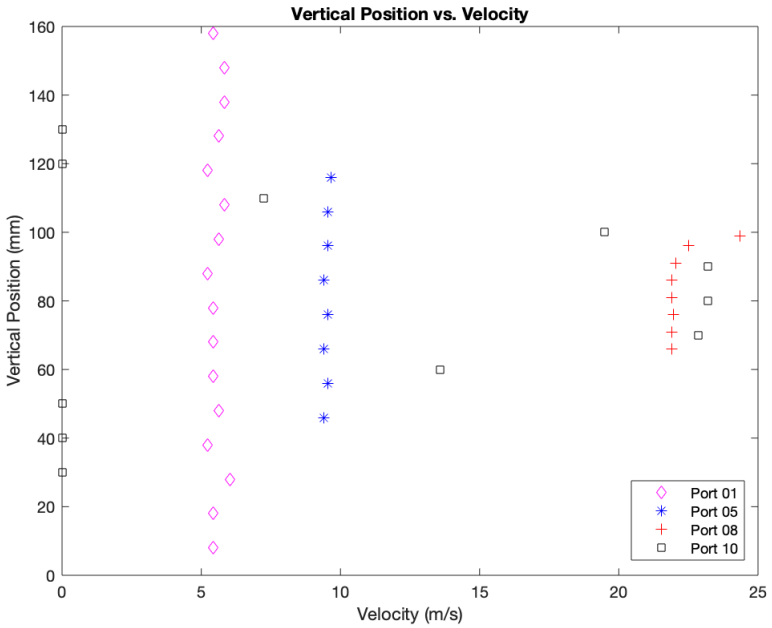

Figure 2: Velocities calculated at different vertical positions for four ports.

Given these values, the flow rate of Port 8 was used to determine the velocities at the remaining ports so that we could assume the flow rate was constant through the wind tunnel. Applying continuity, the velocities were then calculated using this flow rate and the cross-sectional areas that were found using their hydraulic diameters. The hydraulic diameter is four times the area, divided by the perimeter of the cross-section.

Reynold's numbers were also calculated using Eq. 11 for each port, where ρ is the density of air, V_{ave} is the average velocity, D_h is the hydraulic diameter, and μ is the dynamic viscosity of air, measured to be 1.81x10^{-5} $\frac{kg}{ms}$.

Finally, the static and stagnation pressures were also calculated using Eq. 8 and Bernoulli's Eq. 6 with V taken as the average velocity V_{ave}. The calculated values for each port are displayed in Table 1 below.

Table 1: Calculated values of each port throughout the wind tunnel.

Port No.	Average Velocity (m/s)	Reynold's No.	Static Pressure (Pa)	Volumetric Flow Rate (m^3/s)	Stagnation Pressure (Pa)
1	5.555	68503.096	-25.065	0.185	-6.164
2	6.233	63858.779	-29.243	0.185	-5.450
3	7.223	58456.148	-37.598	0.185	-5.644
4	8.437	52962.534	-48.738	0.185	-5.138
5	9.502	46377.078	-62.663	0.185	-7.363
6	13.055	39017.656	-72.411	0.185	31.973
7	18.040	30380.973	-214.447	0.185	-15.112
8	22.195	25649.275	-316.100	0.185	-14.371
9	4.063	80068.648	-336.988	0.185	-326.876
10	10.958	88149.714	-341.166	0.185	-267.619

4 Discussion

At close observation of Figure 2, one can see velocity measurements that are consistent with what was expected for Ports 1, 5, and 8. As the cross-sectional areas decreased, the velocities increased significantly with the expected highest velocities found at the throat of the wind tunnel (Port 8). Noticeably though, the velocities for Port 10, which is the only port tested that lies in the diverging duct, are inconsistent and some data points are along the vertical position axis. The velocities along this axis are not actually zero, but the result of calculating imaginary numbers from the square root in Eq. 9. This accounts for the "jaggedness" observed on the plot at this port. In addition, differences were observed at the conclusion of the experiment in the position of streamers that were attached to the converging and diverging sections. At the converging section, all of the streamers were uniformly pointing and slanting toward the throat, while at the diverging duct they were more inconsistently shaped and curved toward the throat.

In addition, it is important to also note how different the volumetric flow rate of Port 10 was from the others. In the converging section and at the throat, the values were fairly close together while that of Port 10 was calculated to be over three times greater. However, it's likely that the flow rate was not actually this high and rather ties into the observations previously mentioned. One can conclude that while Bernoulli's and continuity were applicable for the converging section and the throat, it fails when the wind tunnel diverges. The failure comes from the assumptions of inviscid, steady, incompressible, and streamline flow, where these are no longer all valid at Port 10. However, noting how the static pressure decreases with decreasing cross-sectional area up until Port 9, we can consider the flow inviscid as this the relationship between pressure and area is consistent with Bernoulli and Continuity. Since we can consider air as incompressible and inviscid, it's likely that the assumptions for steady and streamline flow are what contribute to the inconsistencies seen. Possibilities for this behavior include the crossing/mixing of streamlines and turbulence in the flow. We can see from the calculated Reynold's numbers as well that the flow is partially turbulent before the throat, whose Re is very stable, and then very turbulent in the diverging section (Reynold's numbers greater than 2100 can be considered partially to very turbulent). These calculated values, Figure 2, and the observations of the streamers all suggest that there is more disturbance of air flow and less uniform velocity profiles at the diverging duct, while the opposite is true throughout the converging and throat portions of the wind tunnel where the values found were consistent with the assumptions made to apply Bernoulli's and continuity.

This experiment and the discrepancies observed suggest that the wind tunnel can be improved in a variety of ways to improve accuracy in the diverging duct. For example, instead of sharp corners, it would be more beneficial to have a rounded, cylindrical wind tunnel where the flow will be smoother along the edges. In addition, making the wind tunnel larger in general with greater cross-sectional areas will also help to prevent turbulence.

5 Conclusion

The aim of this experiment was to further our understanding of Bernoulli's Principle and the Continuity Equation in the field of fluid mechanics. This was done using various instruments and the wind tunnel at Boston University, converting our measurements into usable pressure values, and then applying Bernoulli and Continuity to analyze the velocity of air flow. Assuming the air to be inviscid and volumetric flow rate to be constant throughout, the highest velocity of flow was found at the throat of the tunnel, while it decreased with increasing cross-sectional area in the converging and diverging test sections. The Reynold's number and stagnation pressures were also calculated for each port during this experiment. While our findings were consistent with our expectations at the converging duct and throat, the values calculated at the diverging ports ultimately rendered our assumptions of the properties of air invalid. This suggests that at the divergent duct, the flow is not along a streamline or steady since air is still inviscid and incompressible. However, the assumptions required for Bernoulli's were adequate for the calculations along the convergent test sections and at the throat and the Continuity equation could therefore be applied.